Application of Dye-Sensitized Solar Cell Technology in the Tropics: Effects of Air Mass on Device Performance

Otakwa R. V. M.*, Simiyu, J.*, Waita, S. M.* ,Mwabora J. M.*

*Department of Physics, College of Physical and Biological Sciences, University of Nairobi

‡Corresponding Author; Otakwa R. V. M., Department of Physics, College of Physical and Biological Sciences, University of Nairobi, PO Box 30197 – 00100 GPO, Nairobi, KENYA, raphael.makokha@yahoo.com, simiyuj@uonbi.co.ke, swaita@uonbi.co.ke, mwabora@uonbi.co.ke

Received: 09.04.2012 Accepted: 05.06.2012

Abstract- Effects of air mass on the performance of a dye-sensitized solar module (DSSM) have been investigated in a tropical area in Nairobi, Kenya. Outdoor measurements were performed at different times on different days and a series of current-voltage (*I-V*) characterizations carried out at different air mass values and module tilt angles. The module performance parameters: Short circuit current density, (J_{sc}), Open circuit voltage, (V_{oc}), Fill factor, (*FF*) and solar-to-electricity conversion efficiency, (η) were extracted from the *I-V* curves. The module's η and FF increased with air mass while V_{oc} and J_{sc} decreased with increase in AM. The module performed better in the afternoon hours than in the morning hours. The results may be useful in tuning dye-sensitized solar cells for use in the tropics as well as in the design of Net Zero Energy buildings.

Keywords- Dye-sensitized, Performance, Air mass, Net-zero-energy-buildings

1. Introduction

Dye-sensitized solar cells (DSSCs) are cheaper alternatives to the conventional silicon solar cells [1]. Their scalable, self-assembled and bottom-up fabrication processes are economical and ecological, making them attractive and credible alternatives to the conventional solar PV systems [2]. Remarkable advances have been in their fabrication [3-5].

In the tropics, a number of DSSC-related studies have been undertaken, including the effects of nitration on pressed TiO_2 photo electrodes for DSSCs [6], DSSCs fabricated from obliquely DC sputtered TiO_2 films [7], theoretical approaches to the temperature effect on the mobility and transport of photo-injected electrons in DSSCs [8] and [9], effects of the concentration of dopant states in photo-activity in Niobium TiO_2 [10], TiO_2 DSSCs with a hole transport material Ogacho [11] and the Anthocyanin sensitized TiO_2 photo electrochemical solar cells [12].

Lately in Nigeria, Ozuomba and co-workers [13] have fabricated DSSCs using dye extracted from local banana grass, whose performance compare with what has been reported by Law and co-workers [14] as well as Suri and co-workers (2007). Otakwa and co-workers [15] has investigated the effects of radiation intensity and temperature on the performance of DSSCs. These enormous research efforts point to the quest by people in the tropics to have access to cheaper electricity - a goal that has been elusive with the conventional silicon solar devices [16]. In this paper, the effect of air mass and tilt angle on the DSSC performance in the tropics is reported.

2. Materials and Methods

2.1. Basic Theory

The DSSC semiconductor electrochemistry

In DSSCs, the electronic excitation in the dye achieved through light absorption promotes dye molecule into a high energy state associated with the Lowest Unoccupied Molecular Orbital (LUMO). This simultaneously creates an electron deficiency in the low energy state - the Highest Occupied Molecular Orbital (HOMO). Electrons in the

LUMO and HOMO states are separated by a difference in enthalpy (h) [17],

$$\Delta h = \Delta E = E_{LUMO} - E_{HOMO} \quad (1)$$

where,

Δh = change in enthalpy,

ΔE = difference in energy,

E_{LUMO} = energy of the least unoccupied molecular orbital,

E_{HUMO} = energy of the highest occupied molecular orbital.

This exodus of the population of the states from their thermal equilibrium values implies a difference in their chemical potentials (μ), which can be stated as follows:

$$\Delta\mu = \mu LUMO - \mu HOMO \quad (2)$$

where,

$\Delta\mu$ = change in chemical potential,

μ_{LUMO} = chemical potential of the least unoccupied molecular orbital,

μ_{HOMO} = chemical potential of the highest occupied molecular orbital.

Efficient DSSC performance relies on the efficiency of electron injection and dye regeneration. Also, the LUMO energy of the dye should be well above that of the TiO_2 conduction band for efficiency in electron injection. For efficient dye regeneration and sustained photocurrent, the $\Delta\mu$ of the redox couple should be higher than the HOMO energy level of the dye molecules. The maximum voltage of a DSSC under illumination normally corresponds to the difference of the TiO_2 Fermi level (E_F) and the $\Delta\mu$ of the electrolyte.

Nonetheless, the basic operation principle of the DSSC relies on the photo-excitation of the dye molecules. Hence, anything that interferes with access to light for the DSSC affects its performance. The strength of the solar beam incident on the DSSC at a given point and time determines its efficiency in photo-exciting electrons from HOMO level of the dye molecules to the LUMO level as shown by equation (3),

$$TiO2|S + h\nu \leftrightarrow TiO_2|S^*_{LUMO} \quad (3)$$

where,

TiO_2 = the titanium dioxide nanoparticles,

| = the interface

S = the ground state of the dye molecules,

$h\nu$ = the photon energy,

S^*_{LUMO} = the excited state of the least unoccupied molecular orbital of the dye molecule.

Solar beams can be attenuated by absorption and scattering as they enter the earth's atmosphere in an effect known as extinction. Scattering is usually caused by suspended aerosols, which may be diverse in volume, size, form and composition. Depletion of incoming solar irradiance by aerosol-laden atmospheres is referred to as atmospheric turbidity. Its effect on the DSSC device performance at the application sites requires to be considered. Absorption on the other hand is mainly caused by the Ozone layer (O_3), Oxygen (O_2), Nitrogen (N_2), precipitable water vapour (H_2O) and Carbon Dioxide (CO_2).

Apart from N_2 and O_2 which remain more or less constant, the amount of the ozone layer varies with latitude and season [18]. The amount of precipitable water vapour also varies instantaneously based on the local conditions [19]. Carbon dioxide has also been on an alarming increase due to the burning of fossil fuels. The atmospheric refraction of the solar beam by these atmospheric gases makes it take a longer path than is geometrically expected. Optical air mass or simply air mass (*AM*) plays a major role in determining atmospheric refraction [20]. *AM* is the path length traversed by the direct solar radiation as a ratio of the path traversed to a point at sea level when the sun is directly overhead. Studying how solar radiation is attenuated by the atmosphere in terms of the air mass, optical thickness and water vapour is important in understanding how solar devices would perform under different atmospheric settings.

To maximize collected energy, solar collectors are usually tilted to capture maximum radiation. Optimum tilt angle, and hence J_{ph} are influenced by the air mass at a particular place [21]. A number of formulae have been developed for computing *AM*. In this work, the method of erecting a vertical post at a place where the shadow of the post is cast on a flat surface has been used. Dividing the length of the hypotenuse of the triangle (length traversed by the ray of light) (figure 1) by the height of the post yields (geometrically expected path) [22, 23] and applying the Pythagoras theorem yields *AM*,

$$\mathrm{AM} = \left[1 + \left(\frac{s}{h}\right)^2\right]^{1/2} \quad (4)$$

where,

AM = the air mass,

h = the height of the post,

s = the length of the shadow cast by the post.

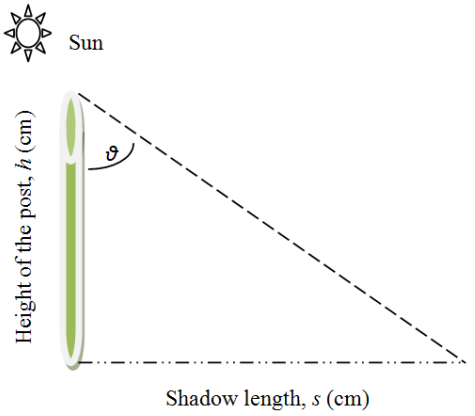

Fig. 1. Illustration on how to determine air mass from the shadow of a vertical post.

From trigonometry, the cosine of θ is obtained by dividing the length adjacent to it by the hypotenuse; the inverse of which constitutes *AM*. This is used for small values of θ.

$$AM=1/(Cos\ \theta) \quad (5)$$

where,

AM = the air mass,

θ = the angle from the vertical.

Equation (5) however assumes a homogenous atmosphere and ignores the earth's curvature. The earth is however not flat and the equation leads to an infinite air mass at the horizons. Kasten and Young [24] developed the equation:

$$AM = [Cos\theta + 0.50572\ (96.07995 - \theta)^{-1.6364}]^{-1} \quad (6)$$

where

AM = the air mass,

θ = the solar zenith angle.

The solar beam available for photo-generation depends on how it is attenuated through the atmosphere. On striking the surface of the DSSC cells, the solar beams eject electrons from the excited dye molecules. These get injected into the conduction band of the TiO_2 as demonstrated by equation (7),

$$S^*_{LUMO} + CB_{TiO_2} \rightarrow TiO_2|S^+ + e_{CB^-} \quad (7)$$

where,

S^*_{LUMO} = the excited state of the least unoccupied molecular orbital of the dye molecule,

CB_{TiO2} = the conduction band of the titanium dioxide semiconductor,

TiO_2 = titanium dioxide,

| = interface

S^+ = oxidized state of the dye molecules,

e_{CB^-} = the electron injected into the conduction band.

The electron then migrates through the TiO_2 nanoparticle network towards the transparent conducting oxide (TCO) substrate. Charge localization due to the polarization of the mediums and relaxation of the molecular ions dominates the physics of charge transfer and transport during these processes. The catalytic reaction at the counter electrode (courtesy of the platinum film) must guarantee fast re-generation of the redox couple as illustrated by [25],

$$Pt + I_3^- \rightarrow 3I^- \quad (8)$$

where,

P_t = the Platinum,

I_3^- = the iodide ions,

$3I^-$ = the iodine ions.

To achieve an efficient DSSC operation, the electron injection rate must be faster than the decay rate. The oxidized dye molecules must also be regenerated fast by the redox couple so as to kinetically compete in the uptake of the electrons from the counter electrode for the subsequent electron injection to prevent recombinations [26]. Also, the rate of reduction of the oxidized sensitizer (S^+) must be higher than the rate of back reaction of the injected electrons as well as the rate of injection of electrons in the electrolyte,

$$TiO_2|S^+ + 3I^- \rightarrow I_3^- + S \quad (9)$$

where,

TiO_2 = the titanium dioxide nanoparticles,

| = interface

S^+ = the oxidized state of the dye molecules,

S = the ground state of the dye molecules,

I_3^- = the iodide ions,

$3I^-$ = the iodine ions.

During these processes, some electrons are not successfully injected into the TiO_2 conduction band due to inadequate energy. They as a result drop back into the HOMO level. The electrons already injected into the conduction band of the TiO_2 risk migrating back into the HOMO level of the dye molecules or into the electrolyte as illustrated by equations (7) and (8) respectively due to electron trapping defects. These result in recombinations that decrease the performance of the cell.

$$e_{CB^-} + S_{HOMO} \rightarrow S + CB_{TiO_2} \quad (10)$$

$$e_{CB^-} + I_3^- \rightarrow 3I^- + CB_{TiO_2} \quad (11)$$

where,

e_{CB^-} = the electron injected into the conduction band.

S_{HOMO} = the ground state of the least highest occupied molecular orbital of the dye molecules,

S = the ground state of the dye molecules,

CB_{TiO2} = the conduction band of the titanium dioxide nanoparticles,

I_3^- = the iodide ions,

$3I^-$ = the iodine ions.

The response of DSSCs under illumination; just as other photovoltaic (PV) devices, is determined by its *J-V* characteristics modelled according to [15],

$$J = J_{ph} - J_s \exp\left[\frac{V+R_sJ}{mV_T}\right] - \sigma V \quad (12)$$

where

J = the ideal current density,

J_{ph} = the photo-generated current density,

J_s = the saturation current density,

V = the voltage across the PV device terminals,

m = the ideality factor,

V_T = the thermal voltage,

R_s = the series resistance,

σ = the shunt conductance.

From equation (9) the photo-generated current density can be plotted as a function of the applied bias voltage. This results in a curve typically known as the current density-voltage (*J-V*) characteristic curve from which key device parameters; open circuit voltage (V_{oc}), short circuit current density (J_{sc}), fill factor (*FF*) can be extracted and efficiency (η) computed.

FF is a measure of the squareness of the *J-V* curve and hence the quality of the solar PV device. It is generally influenced by the series and shunt resistances. It is determined from equation [12],

$$FF = \frac{P_m}{V_{oc}J_{sc}} = \frac{J_{mp}V_{mp}}{V_{oc}J_{sc}} \quad (13)$$

where,

FF = the fill factor,

P_m = the maximum power,

V_{oc} = the open circuit voltage,

J_{sc} = the short circuit current density,

J_{mp} = the current density at maximum power point,

V_{mp} = the voltage at maximum power point.

η describes the overall performance of the DSSC. It is defined as the ratio of P_m to the power of incident radiation (P_{in}), which is given by the equation [27],

$$\eta = \frac{P_m}{P_{in}} = \frac{J_{mp}V_{mp}}{P_{in}} = \frac{V_{oc}J_{sc}FF}{P_{in}} x100\% \quad (14)$$

where,

η = the efficiency,

P_m = the maximum power,

J_{mp} = the current density at maximum power point,

V_{mp} = the voltage at maximum power point,

V_{oc} = the open circuit voltage,

J_{sc} = the short circuit current density,

FF = the fill factor.

2.2. Experimental

Materials

One functional dye-sensitized solar module was used in this study. The module; Omny 11200 outdoor module - model number HS Code 85414090 was used as supplied by G24 Innovations Limited (UK). It was made up of 11 cells, rated 0.5 Watts peak and 8 Volts. The cells were 1.5 inches thick and of a 15.92 cm^2 active area each; bringing the total active area of the module to 175.12 cm^2. The other apparatus used in the study were a tilt-able metal rack supplied by Solargent Limited, Kenya, a Keithley 2400 digital source meter supplied @Workbench (LabVIEW^{TM}) application software supplied by National Instruments Inc., USA, a desktop computer supplied by Hewlett-Packard (HP), Kenya and an IEEE-488 GPIB cable supplied by National Instruments Inc., USA. A protractor and a metre rule supplied by Textbook Centre, Kenya were also used in this work.

J-V characterization at different air mass values

The module was fixed on the tilt-able metal rack as shown in figure 2. The set-up was positioned on the roof-top of the Department of Physics, University of Nairobi at a suitable place where shadows could not be cast on either the module. The module was connected to the Keithley 2400 Source Meter using alligator clips The Keithley source meter was connected to the HP desktop computer via an IEEE-488 GPIB interface. The computer was installed with LabVIEW^{TM} application software.

To determine the air mass at different times, an upright post was erected at a suitable flat place next to the *J-V* characterization experiment. The post's height from the ground surface measured using a metre ruler. The length of the shadow cast by the post was measured simultaneously with the acquisition of the *J-V* characterization curves. *J-V* measurements were at tilts that were varied according to the zenith angles corresponding to the air mass at the different times. The module's performance parameters; V_{oc}, J_{sc}, *FF* and at the different air mass values were extracted from the *J-V* curves and η computed. The set-up was as is illustrated in figures 2 and 3.

Fig. 2. Picture of the set up of the module on the tilt-able metal rack.

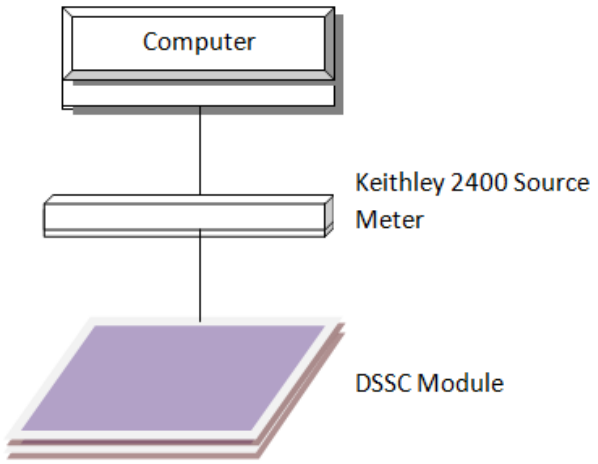

Fig. 3. A simple illustration of the *J-V* characterization experimental set-up.

3. Results and Discussion

From figure 4, it is observed that Voc and Jsc reduced with increase in air mass. This can be attributed to reduction in radiation intensity as air mass increases, which agrees with the observation by Meinel and Meinel [28]. The points at which maximum power is attained (at the 'knee' of the *J-V* curves) increases with air mass. This corresponds to the battery charging region. The fill factor increases with tends to one as air mass increases. This implies that the quality of a DSSC module operating outdoors is best evaluated at higher than lower air mass.

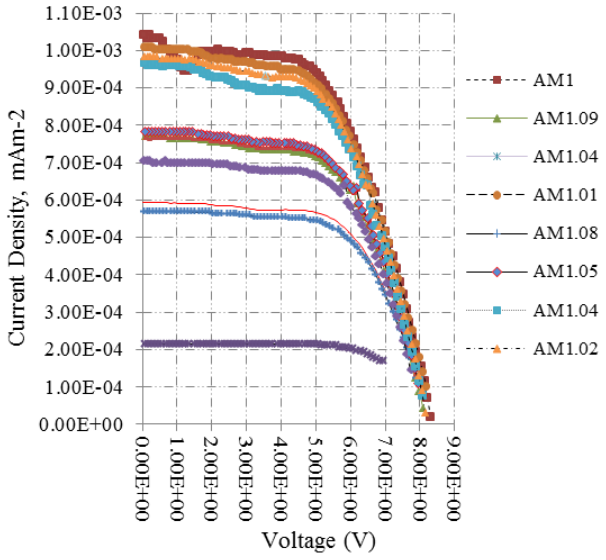

Fig. 4. *J-V* characteristic curves for the module at different air mass values

Air mass varied as shown in figure 5. Values for AM obtained between 700 hours to 1245 hours were slightly unstable compared to the values obtained between 1245 Hours to 1800 Hours. This can be attributed to the instantaneous variation in the atmospheric gaseous absorbers like H_2O, O_2, O_3 and CO_2 as observed by Louche and co-workers [18]. Figure 5 also shows that air mass - and hence the intensity of the direct component of sunlight [28] was more stable in afternoon than in morning hours. V_{oc} and J_{sc} decreased with increase in *AM*.

This can be attributed to the atmospheric extinction of the solar beams due to the longer optical path that they travel through the atmosphere at higher *AM* values. With reduced amount of effective radiation reaching the surface of the module for photo-generation, the photo-generated electrons reduce and consequently, the photo-generated current. The behavior is in agreement with theory, which demonstrates equivalence between photo-generated current density and the corresponding short-circuit current density [15].

Figure 5 also shows how the module's efficiency increased marginally with *AM*. This can be attributed to greater effective radiation available for photo-generation by the module at higher *AM* than at lower *AM*.

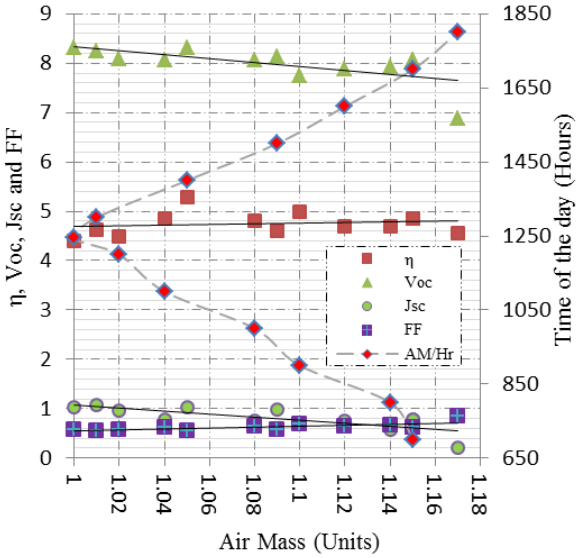

Fig. 5. Curve for Air Mass values at different times of the day.

A comparison of the module's performance in the morning hours and in the afternoon hours is given in figure 6.

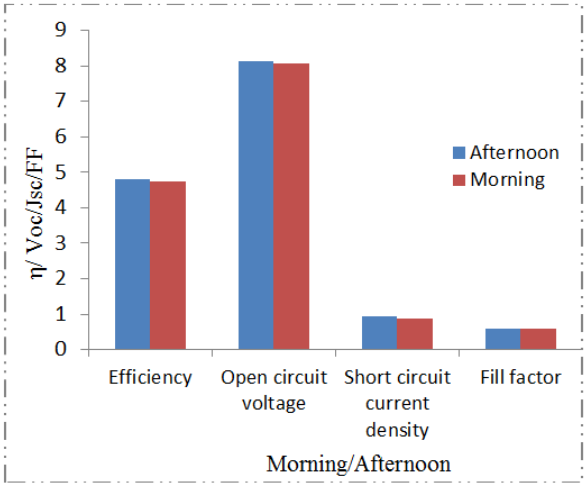

Fig. 6. A chart showing the comparative performance of the module in the morning and in the afternoon.

It is observed that the module performed relatively better in the afternoon hours than in the morning hours. This can be attributed to the more atmospheric turbidity and Railey scattering [24] in morning hours as compared to afternoon hours.

4. Conclusion

The effect of air mass on the performance of a dye-sensitized solar module has been investigated in a tropical area, 1.28˚ South and 35.82˚ East, Nairobi, Kenya. The results show better relative efficiencies for the module at higher air mass. V_{oc} and J_{sc} decreased with increase in air mass. An overall improved performance for the DSSC module was observed in the afternoon hours than in the morning hours. Tuning of DSSCs for use in the tropics may benefit from these finding. The design of energy efficient building facades for the temperate tropics also stands to benefit immensely from these findings.

References

[1] O'Regan, B. and Grätzel, M., (1991). A low cost, high efficiency solar cell based on dye sensitised colloidal TiO_2 films. Nature, 353, p. 737 - 739.

[2] Yum, J., Baranoff, E., Wenger, S., Nazeeruddin, Md. and Grätzel, M., (2010). Panchromatic engineering for dye sensitized solar cells. Energy and Environmental Science, 4 p. 842.

[3] Han, L., Islam, A., Chen, H., Malapaka, C., Chiranjeevi, B., Zhang, S., Yang, X. and Yanagida, M., (2012). High efficiency dye sensitized solar cell with a novel co-adsorbent. Energy and Environmental Science,

[4] Yu, Q., Yu, C., Guo, F., Wang, J., Jioa, S., Gao, S., Li, H. and Zhao, L., (2012). A stable and efficient quasi-solid-state dye-sensitized solar cell with a low molecular weight organic gelator. Energy and Environmental Science, DOI: 10.1039/c2ee03128k, p. 1-5.

[5] Qingjiang, Y., Cuiling, Y., Fengyun, G., Jinzhong, W., Shujie, J., Shiyong, G., Hongtao, L. and Liancheng, Z., (2012). Astable and efficient quasi-solid-state dye-sensitized solar cell with a low molecular weight organic gelator. Energy and Environmental Science, DOI: 10.1039/c2ee03128k.

[6] Wafula, H., (2007). Effects of nitration on pressed TiO2 photoelectrodes for dye-sensitized solar cells. M.Sc. thesis for the Department of Physics, University of Nairobi.

[7] Waita, S., (2008). Dye-sensitized solar cells fabricated from obliquely sputtered nanoporous TiO_2 thin films: characterization, electron transport and lifetime studies. Ph.D thesis for the Department of Physics, University of Nairobi.

[8] Kahuthu, S., (2008). Theoretical approach to the transport phenomenon of photo injected electrons in dye-sensitized solar cells. M.Sc. thesis for the University of Nairobi.

[9] Olwendo, J., (2008). A theoretical approach to studies of temperature effect on mobility of photo injected electrons in dye-sensitized solar cells. M.Sc. thesis for the Department of Physics, University of Nairobi.

[10] Ajuoga, P., (2009). Effects of concentration on dopant states in photo activity in Niobium doped TiO2. M.Sc. thesis for the Department of Physics, University of Nairobi.

[11] Ogacho, A., (2010). A study of TiO_2 dye-sensitized solar cells with a hole transport material. Ph.D thesis for the Department of Physics, University of Nairobi.

[12] Simiyu, J., (2010). Characterization of Anthocyanin Dyes and Investigation of Charge Transport in TiO_2 Dye Sensitized Solar Cells. Ph.D. thesis for the University of Nairobi, p. 1 - 137.

[13] Ozuomba, J., Ekpunobi, A. and Ekwo, P., (2011). The photovoltaic performance of dye-sensitized solar cell based on Chlorin local dye. Chalcogenide Letters, 8 (3), p. 155 - 161.

[14] Law, M., Green, L., Johnson, J. Saykally, R. and Yang, P., (2005). Nanowire dye-sensitized solar cells. Nature Materilas, 4 (6) p. 455 - 459.

[15] Otakwa, R. V. M., Simiyu, J., Waita, S. M. and Mwabora, J. M., (2012). Application of dye-sensitized solar cell technology in the tropics: Effects of radiation intensity and temperature on DSSC performance. International Journal of Advanced Renewable Energy Research (IJARER), 1 (2), p. 17 - 25.

[16] Bakas, I., (2011). Solar energy/photovoltaics. In solar energy and housing - Corpus. Copenhagen Resource Institute (CRI), p. 1 - 6.

[17] Bisquert, J., Cahen, D., Hodes, G., Rühle, S. and Zaban, A., (2004). Physical chemical principles of photovoltaic conversion with nanopartuculate, mesoporous dye-sensitized solar cells. Journal of Physical Chemistry, 108, p. 8106 - 8118.

[18] Louche, A., Maurel, M., Simonnot, G., Peri, G. and Iqbal, M., (2000). Determination of Ăngstrŏm's turbidity coefficient from direct total solar irradiance measurements. Laboratoire d'Hẽlioẽnergẽtique, p. 1622 - 1630.

[19] Iqba, M., (1987). Determination of Ăngstrŏm's turbidity coefficient from direct total solar irradiance measurements. Solar Energy, 38, p. 89 - 96.

[20] Young, A., (1994). Air mass and refraction. Applied optics. 33, p. 1108 - 1110.

[21] Heinemann, D., (2000). Energy meteorology. In lecture notes for the postgraduate programme 'Renewable Energy'. Carl Von Ossietzky Universitat, p. 1 - 102.

[22] Chambers, P., (1999). Teaching Pythagoras' theorem. In mathematics in school, The Mathematical Association, Leicester, 28 (4), p. 22 - 24.

[23] Wenham, S., Green, M., Watt, M. and Corkish, R., (2007). Applied photovoltaics. T J International Ltd., p. 6.

[24] Kasten, F. and Young, A., (1989). Revised optical air mass tables and approximation formula. Applied Optics, 28 (22), p. 4735 - 4738.

[25] Kalagnan, G. and Kang, Y., (2006). A review on mass transport in dye-sensitized solar cells. Journal of Photochemistry and Photobiology C: Photochemistry Reviews, 7, p. 17 - 22.

[26] Thavasi, V., Renugopalakrishnan, V., Jose, R. and Ramakrishna, S., (2009). Controlled electron injection and transport in material interfaces in dye-sensitized solar cells. Materials Science and Engineering: Reports, 63, p. 81 - 99.

[27] Hedegus, S. and Shafarman, N., (2004). Thin film solar cells: Device Measurement and Analysis. Progress in Photovoltaic Research and Application, 12, 155-176.

[28] Meinel, A. and Meinel, M., (1976). Applied solar energy. Addison Wesley Publishing Company,